Proceedings Paper:
Mao, M, Zhang, L, Musembi, M et al. (2 more authors) (2018) Artificial Fish Swarm Algorithm Based-Maximum Power Generation for Grid-Connected PV Panels. In: 2017 UKSim-AMSS 19th International Conference on Modelling & Simulation. UKSim 2017, 05-07 Apr 2017, Cambridge, UK. Institute of Electrical and Electronics Engineers (IEEE) , pp. 149-154. ISBN 978-1-5386-2735-8

https://doi.org/10.1109/UKSim.2017.13

Artificial Fish Swarm Algorithm Based-Maximum Power Generation for Grid-Connected PV Panels

Mingxuan Mao[1,2]
[1]Automation College
Chongqing University
Chongqing, China
Email: mx_m@cqu.edu.cn

Li Zhang
[2]School of Electrical and Electronic Engineering
University of Leeds
Leeds, United Kingdom
Email: L.zhang@leeds.ac.uk

Mark Musembi, Benjamin Chong
School of Electrical and Electronic Engineering
University of Leeds
Leeds, United Kingdom

Qichang Duan
Automation College
Chongqing University
Chongqing, China

Abstract—This paper proposes a novel maximum power point tracking (MPPT) method and a single-phase grid-connected photovoltaic (PV) system using a half-bridge active neutral point clamped (ANPC) inverter. The new MPPT method uses a modified artificial fish swarm algorithm (MAFSA) performed by a boost DC/DC converter. For the ANPC a switching-loss balancing pulse-width modulation scheme is used for control of the inverter. This scheme has shown to increase the maximum power point searching speed and accuracy, and by combining this tracking technique with the inverter, the overall system efficiency is higher the conventional particle swarm optimization (PSO) based-MPPT method. The performance of the proposed system is verified through simulation studies under the different partial shading conditions.

Keywords-PV system; grid connection; ANPC; MAFSA; MPPT

I. INTRODUCTION

PV power generation for domestic applications is commonly performed in single-phase, grid-connected methods and the system is required to be of low cost, high efficiency and offer long lifetimes [1]. The transformerless inverter provides a small footprint, highly efficient way of achieving this, although at the cost of leakage current susceptibility. Specialized transformerless inverter topologies which minimize the leakage current between the PV panel and grid have been developed. These include full-bridge (FB) derived topologies such as the H5, HERIC, REFU and FB-DCBP converters, as well as Neutral Point Clamped (NPC) derived topologies such as the NPC half-bridge, Conergy NPC and Active NPC (ANPC) converters [2]. The conventional half-bridge NPC converter suffers from the disadvantage that the losses among its switching devices are unbalanced [3]. This limits the output power of the converter to the maximum permissible losses of the highest-loss devices, and so in an effort to mitigate this the ANPC inverter was proposed [4]. In addition to grid-connection, the PV power generator is required to maintain high-efficiency operation, i.e. ensuring maximum power harvesting throughout. Some studies have addressed that conventional MPPTs are operated on a sensing current. There exist some commercially well-known MPPTs such as perturb and observe (P&O) [5], incremental conductance (INC) [6] and hill climbing (HC) [7]. In addition, soft-computing techniques have been catching the interest of researchers due to their effectiveness, low cost, robustness and global peak searching capability. Especially, the conventional MPPT techniques fail to guarantee successful tracking of the global MPP under partial shading conditions, resulting in significant reduction of both the generated power and the PV energy production system reliability. Based on this background, the soft-computing techniques are catching the interest of researchers due to their effective, low cost, robustness and their global peak search capability [8].

This paper proposes a single-phase PV grid-connected system which comprises a PV panel with a boost converter for MPPT and an ANPC for grid connection as shown in Fig. 1. A modified artificial fish swarm algorithm (MAFSA) is proposed which incorporates a region-checking scheme to determine the location of the operating point in relation to the MPP based on the power and voltage (P-V) characteristic of a PV panel. The proposed MPPT algorithm combines the searching capabilities of the Particle Swarm Optimization (PSO) and the self-learning ability of adaptive visual and step for the basic artificial fish swarm algorithm (AFSA), which leads to quick and accurate search for the MPP and hence resulting in reduction of the voltage ripple and imcresed power output.

Combining the PV section with the ANPC inverter for grid connection, the PWM strategy employed for the control of the inverter is the double-frequency PWM (DF-PWM) [9] which increases the switching states of the inverter thus leading to re-distribution and balancing of the switching-loss among the devices. The details of the above will be described. Simulation studies of the whole system under different incident levels have been carried out, the results demonstrating the features and merits of the scheme will be presented.

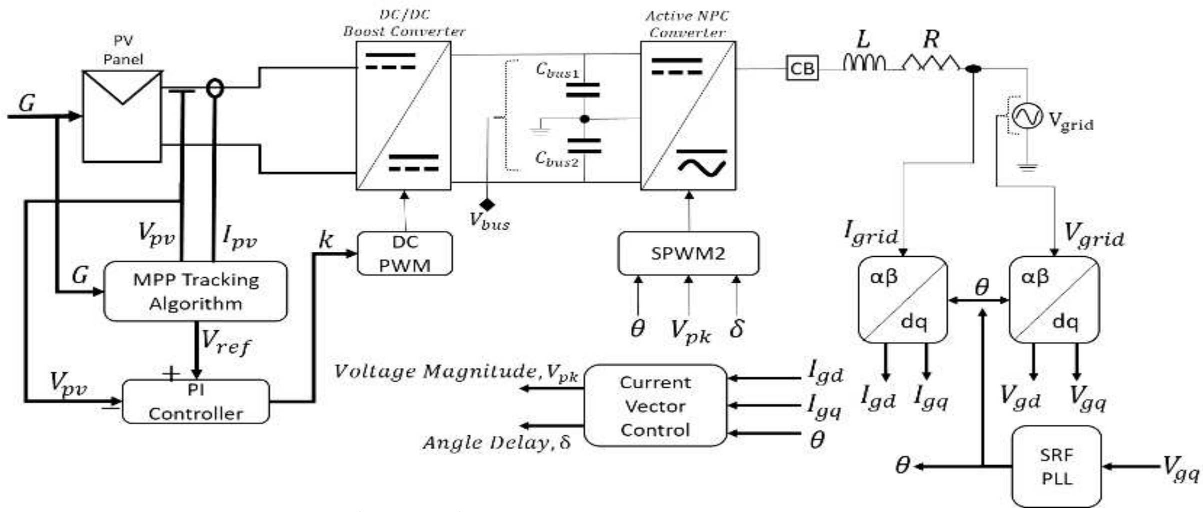

Figure 1. Configuration of the proposed PV grid-connected system with ANPC inverter

II. MODIFIED ARTIFICIAL FISH SWARM ALGORITHM BASED-MPPT ALGORITHM

A. The basic PSO algorithm

The standard PSO [8] algorithm is shown as follows:

$$v_{t+1} = \omega v_t + \alpha_t^l \left(p_t^l - x_t \right) + \alpha_t^g \left(p_t^g - x_t \right) \tag{1}$$

$$x_{t+1} = x_t + v_{t+1} \tag{2}$$

where subscript t denotes the index of iteration; v_t represents the speed of the particle in the t^{th} iterative process; x_t represents the speed of the particle in the t^{th} iterative process; p_t^l represents the current individual extreme value point of the particle in the t^{th} iterative process; p_t^g represents the current global extreme value point of the population in the t^{th} iterative process; ω is known as the inertia weight; c_1 and c_2 are treated as the acceleration factors, and $\alpha_t^l= c_1r_1$, $\alpha_t^g= c_2r_2$, r_1, r_2~U(0,1), ω, α_t^l, $\alpha_t^g \in$R, α_t^l~U(0,c_1), α_t^g~U(0,c_2).

B. AFSA optimized by PSO algorithm

Being attracted by the potential of AFSA, a lot of improved algorithms based on the ordinary AFSA have been proposed, such as the introduction of taboo optimization operator [10], the introduction of the fish jumping behavior [11] and the introduction of fish memory behavior [12]. In the proposed algorithm, the various characteristics of PSO algorithm, including speed inertia, the memory (learning) of individual particle, and information exchange and sharing between particles, respectively are introduced into the AFSA. The improvements of the AFSA with PSO are expressed as follows:

At first, the speed parameter is introduced into each of the artificial fishes. Taking the swarm behavior for example, the updated speed formula can be represented as follows:

$$V_{t+1} = \omega V_t + \text{rand} \times \frac{\text{Step}_i \times (X_t^c - X_t)}{\text{norm}(X_t^c - X_t)} \tag{3}$$

where ω is the inertia weight; v_t represents the velocity vector of the artificial fish in the t^{th} iterative process; Step is the largest mobile step length; X_t^c is the center of the cluster behavior vector; X_t represents the current position vector of the artificial fish in the t^{th} iterative process; norm (X_t^c-X_t) represents the distance between the two position vector, and rand~ U (0, 1).

Secondly, the memory behavior pattern is introduced. This behavior makes the artificial fish in swimming refer to its own optimal position, which can reduce the blindness of the fish in the search process. The updated speed is shown as follows:

$$V_{t+1} = \omega V_t + \text{rand} \times \frac{\text{Step}_i \times [\xi_t (X_t^{pbest} - X_t)]}{\text{norm}[\xi_t (X_t^{pbest} - X_t)]} \tag{4}$$

where X_t^{pbest} represents the optimal position vector of the artificial fish on the bulletin board in the t^{th} iterative process; X_{t-1}^{pbest} represents the optimal position vector of the artificial fish on the bulletin board in the t-1^{th} iterative process.

Thirdly, the communication behavior pattern is introduced. This behavior makes the artificial fish in swimming refer to the optimal position of the whole fish, which strengthens the ability of exchanging and sharing information between the individual in the search process, and further reduces the blindness of the fish in the search process. The updated velocity is shown as follows:

$$V_{t+1} = \omega V_t + \text{rand} \times \frac{\text{Step}_i \times [\xi_t (X_t^{gbest} - X_t)]}{\text{norm}[\xi_t (X_t^{gbest} - X_t)]} \tag{5}$$

where X_t^{gbest} represents the current global extreme value point of the population on the bulletin board in the t^{th} iterative process; X_{t-1}^{gbest} represents the current global extreme value point of the population on the bulletin board in the t-1^{th} iterative process.

C. The proposed algorithm

Visual and step are two very important parameters for AFSA, and have important effect on the optimization result. When visual and step are set to the greater value for artificial fish, although artificial fish are provided with high search capacity and fast convergence in the previous stage, artificial fish will inevitably oscillate back and forth in the vicinity of the optimal value in the late of convergence. On the contrary, artificial fish can improve convergence precision, but artificial fish are very easy to fall into the local optimal value when the local optimal value is prominent. So, it is necessary that visual and step of artificial fish can be adaptively calculated along with the iteration [13].

In MAFSA, each artificial fish is in local neighborhood structure. Before each of iteration, the distance between the ith of artificial fish and the other 5 neighbor artificial fish need to be calculated. Visual and step is dynamically defined as follows [13]:

$$\begin{cases} Visual_i = K_1 * \frac{1}{3} * \alpha(t) * \sum_{j=1}^{3} d_{i,j} + Visual_{min} \\ Step_i = \frac{1}{8} * \alpha(t) * Visual_i + Step_{min} \\ \alpha(t) = \exp(-K_2 * (t / TolalIter)^2) \end{cases} \tag{6}$$

where K_1 is a uniform random number within the range (0, 1) and its value is relative to the search range and dimension of the optimized function; $\alpha(t)$ represents the relationship between visual, step and the number of iteration; $Visual_{min}$ represents the minimum of visual; $Step_{min}$ represents the minimum of step; K_2 represents the limited factor; t represents the current number of iterations; VisualIter is the total number of iterations.

Furthermore, the maximum distance (MaxD) is used to limit the minimum length of vision and step of the fish dynamically, which two random fishes may appear to be in the D dimension search space. In addition, MaxD is shown as follows.

$$MaxD = \sqrt{(x_{max} - x_{min})^2 \times D} \tag{7}$$

where x_{max} and x_{min} respectively represent the upper and lower bound of the optimization range, D is the dimension of search space; $Visual_{min}$ is set to MaxD/100; $Step_{min}$ is set to MaxD/500.

D. The proposed method for global MPPT of PV array under PSCs

Taking the branch current as the optimization variables, the fitness function is P-I relationship of the series branch, as shown in formula (8) and formula (9).

$$fit = I \times \sum_{k=1}^{n_s} PVprog(i_k, Sun_k, T_k), n_z = 10 \tag{8}$$

$$PVprog(I, Sun, T) = 1.1103 \times \log_{10} \left(\frac{3.8 \times Sun - I + 2.2 \times 10^{-8}}{2.2 \times 10^{-8}}\right) - 0.2844 \times I \tag{9}$$

where PVprog(I, Sun, T) represents the output power of each of PV panels-current characteristic function, Sun and T respectively represent light intensity and environment temperature.

The specific process of the proposed MPPT algorithm is shown as follows:

a) Initialize the position and speed of the fish, the optimal locations of each fish's memory and the optimal position parameters recorded on bulletin board;

b) Test the 4 kinds of combination behavior patterns: cluster or foraging, collision or foraging, memory or foraging and communication or foraging;

c) Select the optimal combination behavior model from b) and use the velocity update current location of the artificial fish;

d) If the specified number of iterations is available, the optimization will end, otherwise going to step b).

Furthermore, the flowchart of the proposed algorithm is shown in Fig. 2.

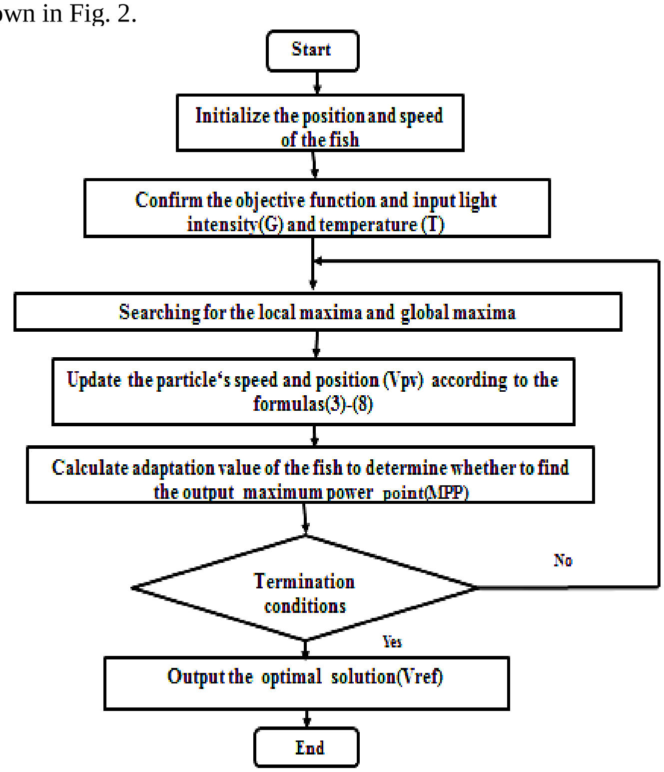

Figure 2. Flowchart of MAFSA-based MPPT algorithm

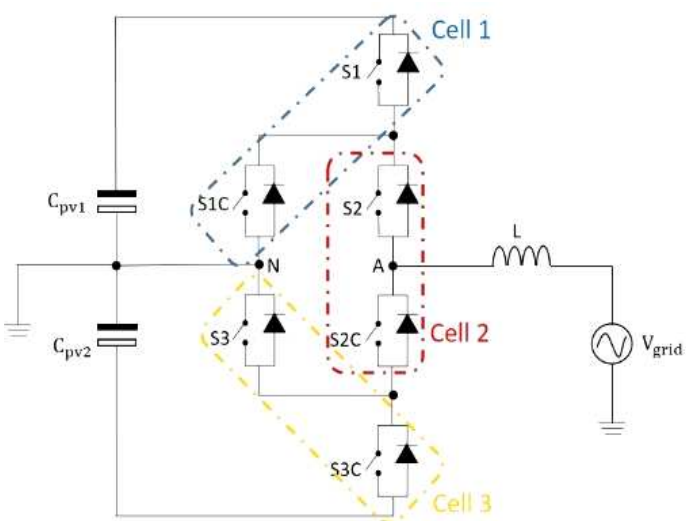

Figure 3. ANPC converter structure

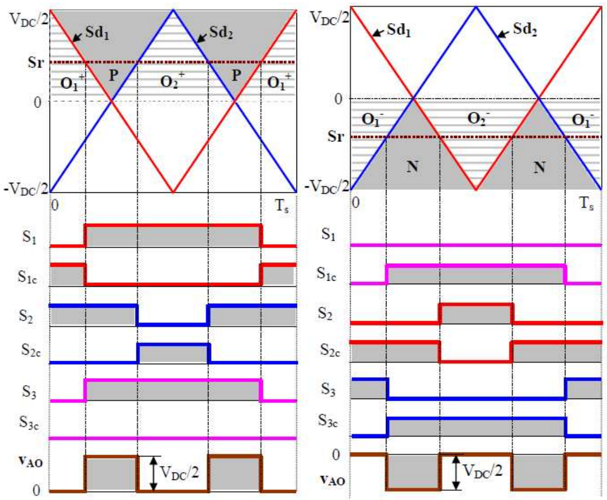

Figure 4. DF-PWM switching signals for ANPC converter

III. ANPC GRID-CONNECTED INVERTER AND ITS PWM SCHEME

A. ANPC Inverter

The 3-level ANPC converter is derived from the 3-level NPC converter, with the neutral-point clamping diodes replaced by bidirectional switches as shown in Fig. 3 [9]. The ANPC switches are required to withstand a voltage magnitude of $V_{DC}/2$.

The ANPC converter switches can be grouped in a 3-cell configuration corresponding to the duty cycle imposed on each cell by the PWM [9]. The ANPC converter does not improve the total efficiency of the NPC converter, but rather improves the performance by re-distributing losses across the switching devices, reducing stress on them. Introducing more zero-voltage states (ZVS) makes it possible to distribute the conduction losses, by cycling between the upper conduction path, where switches S1C and S2 conduct, and the lower path, where switches S3 and S2C conduct. During the positive or negative voltage states, however, the conduction losses cannot be influenced [9]. The switching losses of the converter are influenced by the commutation between positive or negative states and the ZVS. As such, it is possible to redistribute the converter switching losses by controlling the ZVS conduction paths [9] [3].

B. Double-Frequency PWM

The DF-PWM strategy is introduced in [3] and [9] and is a PWM strategy where the apparent switching frequency is doubled at the converter output. The converter has a total of six states, with four zero-voltage states. This PWM scheme makes use of two carrier waveforms phase-shifted by half a cycle and one sinusoidal control waveform. The achieved switching signals over one switching period are shown in the Fig. 4, for the positive and negative cycles of the control waveform [9]. As shown, the output voltage has an apparent frequency twice the switching frequency. Switches S_2 and S_{2C} utilize the original carrier waveform while the switches S_1, S_{1C}, S_3 and S_{3C} utilize the phase-shifted carrier waveform. The positive voltage state is obtained when switches S_1, S_2 and S_3 are all on, while the negative voltage state is obtained when switches S_{1C}, S_{2C} and S_{3C} are all on [9]. There are two ZVS per active voltage state, giving four in total. During the positive reference state, the first ZVS utilizing the upper conduction path is obtained when switches S_{1C}, and S_2 are on. The second utilizing the lower conduction path is obtained when switches S_1, S_{2C} and S_3 are on. During the negative reference state, the ZVS utilizing the upper conduction path is obtained when switches S_{1C}, S_2 and S_{3C} are on while that utilizing the lower conduction path is obtained when switches S_{2C}, and S_3 are on. The current paths during both the positive and negative voltage reference states are similar for the upper and lower conduction paths respectively [9]. The DF-PWM scheme commutation occurs such that the two possible ZVS per active reference state are equally utilized. The converter commutation action is shown in Fig. 5.

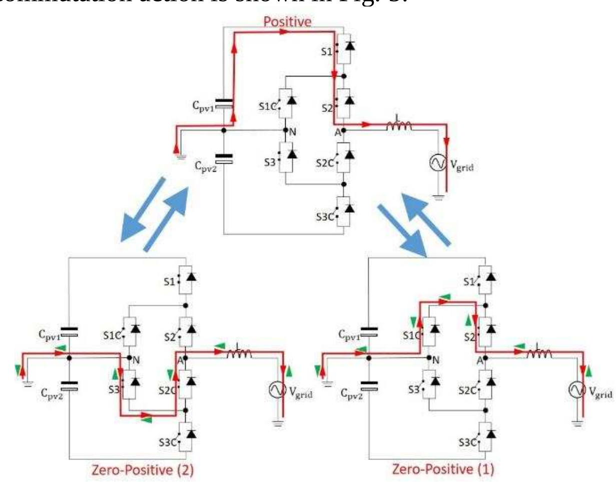

(a)

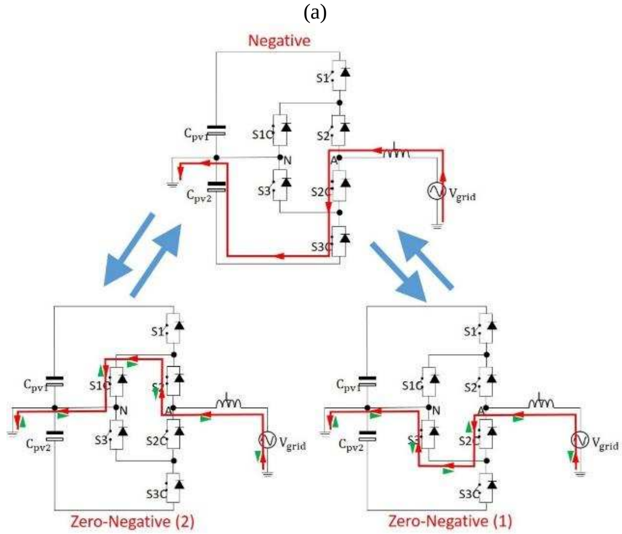

(b)

Figure 5. ANPC inverter commutation action between positive, negative and zero states: (a) positive, and (b) negative

IV. SIMULATION OF PV GRID-CONNECTED SYSTEM WITH ANPC INVERTER

The grid-connected converter and the MPP controlled PV array (2 modules) with boost converter were integrated into a single system for simulation. In addition, the PV array consists of two modules and the parameters of module are shown in Table I. To simulate the different shading situation for the PV array, the insolation of the second PV panel occurs to change suddenly from 600W/m^2 to 800W/m^2 at 0.5s, from 800W/m^2 to 500W/m^2 at 1s, from 500W/m^2 to 1000W/m^2 at 1.5s and from 1000W/m^2 to 700W/m^2 at 2s, in the whole process of simulation. The aim of the simulation was to observe the variation of harvested PV power with changes in irradiation, as well as compare it to the power injected into the grid by the ANPC converter. The Simulink block diagram of the system is shown in Fig. 6, and the simulation parameters of the system are given in Table I. Table II shows the basic parameters of the traditional PSO method and the proposed method.

TABLE I. SYSTEM PARAMETERS USED IN THE SIMULATION

PV modules	33 W at 25ºC, 1kW/m^2
DC bus voltage	80 V
DC bus capacitors	2 mF
Output inductor	4.5 mH
Output resistor	0.1 Ω
Grid voltage	32.5 V_{rms}
Grid frequency	50 Hz

TABLE II. PARAMETERS OF THE ALGORITHMS

Algorithm	Parameter	Value
PSO	ω	[0.9 , 0.4]
	$c_1 = c_2$	2
MAFSA	$\xi_t = \xi_{t-1}$	0.5
	K_1	1/20
	K_2	30
	$Visual_{min}$	MaxD/100
	$Step_{min}$	MaxD/500
	Try_number	5
	δ	0.75

A quadrature signal based phase locked loop using a quarter-cycle delay was implemented in the system for synchronization of the AC inverter current to the grid voltage. In order to control the power injected into the grid and keep the DC-bus voltage constant, a current vector controller was implemented in the system as shown in the system diagram in Fig. 1 and Fig. 6. The PV power output variation with changes in irradiation is presented in Fig. 7, and shows the variation of inverter output current with changes in incident irradiation, as well as the PV panel output power and the power injected into the grid for both the basic PSO and the proposed MAFSA. The control strategies of the inverter are shown to be functional as the grid-injected power follows the PV-produced power closely. It can be noted from Fig. 7 that the grid-injected power is more stable and shows less ripple for the proposed method than that of the conventional PSO.

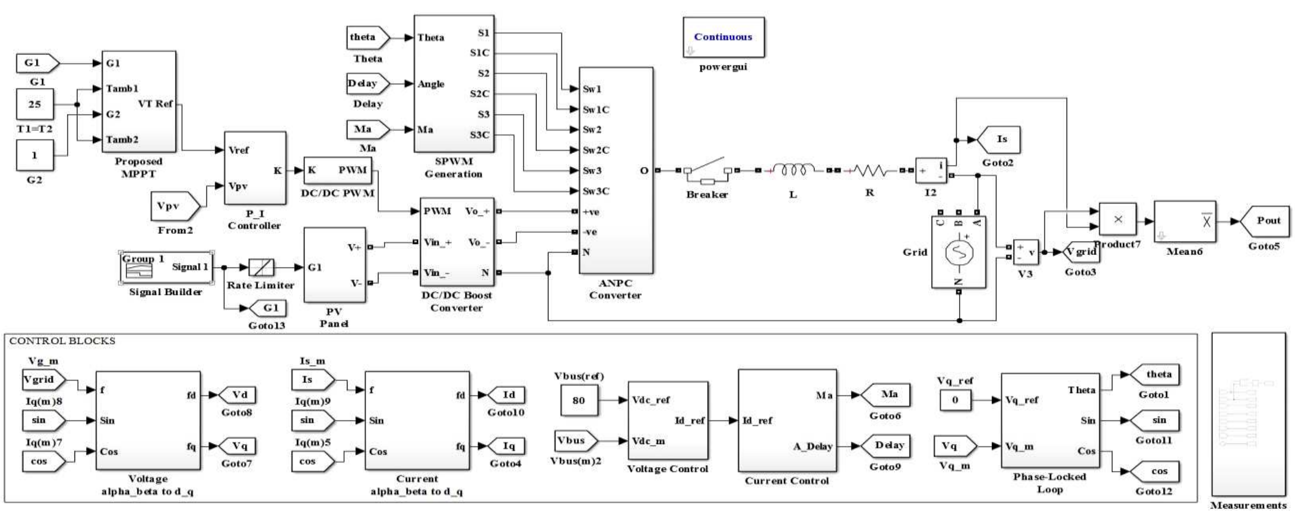

Figure 6. Simulink block diagram of the grid-connected system

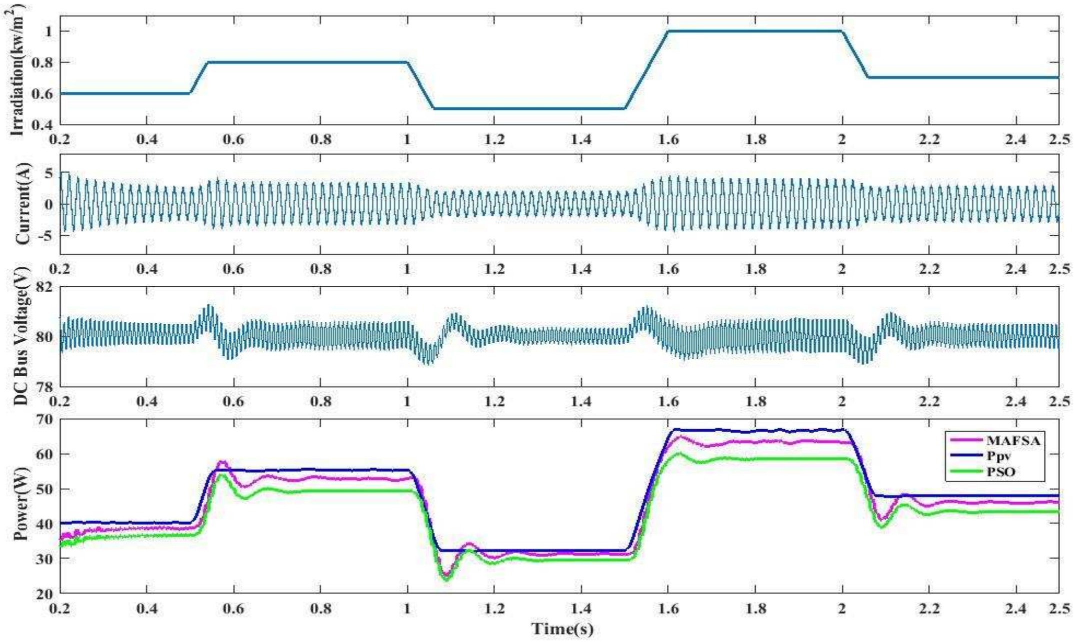

Figure 7. Plot showing, from top, (a) variation of incident irradiation, (b) variation of inverter output current, (c) DC bus voltage variation at the ANPC converter input, and (d) PV panel power output (Ppv) (blue), inverter output power with the basic PSO (green) and inverter output power with MAFSA (pink)

ACKNOWLEDGMENT

This work has been supported by the National Natural Science Foundation of China (Grant No. 51377187), the Graduate Scientific Research and Innovation Foundation of Chongqing (Grant No.CYB16048) and the China Scholarship Council (CSC).

REFERENCES

[1] F. Blaabjerg, F. Iov, T. Kerekes, and R. Teodorescu, "Trends in power electronics and control of renewable energy systems," Proceedings of 14th International Power Electronics and Motion Control Conference EPE-PEMC 2010, Sep. 2010.

[2] N. Mohan, T. M. Undeland, W. P. Robbins, and T. M. Undel, Power electronics: Converters, applications and design, media enhanced, 3rd ed. United States: John Wiley and Sons (WIE), 2003.

[3] T. Bruckner, S. Bernet, and P. K. Steimer, "The active NPC converter for medium-voltage applications," Fourtieth IAS Annual Meeting. Conference Record of the 2005 Industry Applications Conference, 2005.

[4] T. Bruckner, S. Bernet, and H. Guldner, "The active NPC converter and its loss-balancing control," IEEE Transactions on Industrial Electronics, vol. 52, no. 3, pp. 855–868, Jun. 2005.

[5] N. Femia, G. Petrone, G. Spagnuolo, and M. Vitelli, "Optimization of perturb and observe maximum power point tracking method," IEEE Trans. Power Electron., vol. 20, no. 4, pp. 963-973, 2005.

[6] A. Safari, and S. Mekhilef, "Simulation and hardware implementation of incremental conductance MPPT with direct control method using cuk converter," IEEE Trans. Ind. Electron., vol. 58, no. 4, pp. 1154–1161, 2011.

[7] B. N. Alajmi, K. H. Ahmed, S. J. Finney, and B. W. Williams, "Fuzzy-logic-control approach of a modified hill-climbing method for maximum power in micro grid standalone PV systems," IEEE Trans. Power Electron., vol. 26, no. 4, pp. 1022-1030, 2011.

[8] K. Ishaque, Z. Salam, M. Amjad, and S. Mekhilef, "An improved particle swarm optimization (PSO)–based MPPT for PV with reduced steady-state oscillation," IEEE Trans. Power Electron., vol. 27, no. 8, pp. 3627–3638, 2012.

[9] D. Floricau, E. Floricau, and M. Dumitrescu, "Natural doubling of the apparent switching frequency using three-level ANPC converter," 2008 International School on Nonsinusoidal Currents and Compensation, Jun. 2008.

[10] Y. Yu,Y. F. Tian and Z. F. Yin. "Multiuser detector based on adaptive artificial fish school algorithm," In: Proceeding of IEEE International Symposium on Communications and Information Technology, Beijing, China,1480-1484, 2005.

[11] C. R. Wang, C. L. Zhou and J. W. Ma. "An improved artificial fish-swarm algorithm and its application in feed-forward neural networks," In: Proceeding of the 4th International Conference on Machine Learning and Cybernetics, Guangzhou, China, 2890-2894, 2005.

[12] H. C. Tsai and Y. H. Lin. "Modification of the fish swarm algorithm with particle swarm optimization formulation and communication behavior," Appl. Soft Comput., vol. 11, no. 8, pp. 5367-5374, 2011.

[13] H.Y. Xu, W.B. Sun, X. Zhang, H.J. Niu, and C.L. Bai. "Local neighborhood artificial fish swarm algorithm based on adaptive visual and step," Comp. Eng. and Des. vol. 33, no. 7, pp. 2815-2821, 2012.